Plasmonics (2019) 14:79–89
https://doi.org/10.1007/s11468-018-0780-9

# Photocatalytic Properties under Sunlight of Heterostructures AgCl/CuO Obtained by Sonochemical Method

N. F. Andrade Neto[1] · E. Longo[2] · K. N. Matsui[3] · C. A. Paskocimas[1] · M. R. D. Bomio[1] · F. V. Motta[1]

Received: 14 March 2018 / Accepted: 28 May 2018 / Published online: 13 June 2018


**Abstract**
AgCl/CuO heterostructures were synthesized via a sonochemical method. AgCl/CuO molar compositions of 1:1 and 2:1 were prepared, respectively. Such compositions were prepared using three distinct routes. The particles were characterized by X-ray diffraction (XRD), scanning electron microscopy (SEM-FEG) and UV-Vis spectroscopy (UV-Vis). In order to analyze the applicability of the heterostructure, photocatalytic tests were performed under sunlight and UV-Vis radiation for the degradation of the methylene blue dye. The results of the X-ray diffraction confirmed the formation of the AgCl/CuO heterostructure in all samples, with no evidence of doping or formation of deleterious phases. SEM images indicate a cubic-like morphology for the AgCl particles, forming $Ag^0$ on its surface, the CuO particles have a leaf appearance. The results of the photocatalytic activity indicate that the increase of the AgCl molar ratio from 1:1 to 2:1 accelerates the degradation of methylene blue for both the radiations and shows that sunlight decreases by at least 55% for the degradation of the methylene blue, depending on the composition, to the heterostructure.

**Keywords** Photocatalysis · Sunlight · Heterostructure · AgCl/CuO · Sonochemical

## Introduction

The literature reports that copper and its compounds have been applied as water-sterilizing agents, avoiding the proliferation of microorganisms and associated problems [1–4]. The shape, size, and positive charges on the surface of the particles facilitate the negative bacterial surface binding, resulting in a better bactericidal effect [1, 2]. In the photocatalytic processes using semiconductors, under light radiation, an electron is excited from the valence band to the conduction band, such excitation promotes the generation of a hole in the valence band, where it interacts with $H_2O$ or $OH^-$, which are adsorbed on the band (OH), or the electron excited for the conduction band interacts with the $O_2$ adsorbed, generating $O_2^-$ [5].

✉ N. F. Andrade Neto
nfandraden@gmail.com

[1] LSQM, DEMAT, UFRN, Av. Sen. Salgado Filho, 3000, Natal, RN 59072-970, Brazil

[2] LIEC, DQ, UFSCar, Via Washington Luiz, km 235, São Carlos, SP 13565-905, Brazil

[3] LabCQ, DEQ, UFRN, Av. Sen. Salgado Filho, 3000, Natal, RN 59072-970, Brazil

Copper oxide has gained a lot of attention in photocatalytic activity because it has a small bandgap (~ 1.2 eV). Silver particles have received great attention in the last decades in the fields of engineering due to their wide field of application, as for example in the catalysis [6], fuel cells [7], and lithium batteries [8]. The effect of silver on antimicrobial activity has also been gaining attention. Ibanesco et al. [9] impregnated silver nanoparticles in ZnO, and with their increase, it also increased antimicrobial capacity against *Escherichia coli* and *Micrococcus luteus* bacteria. Metal particles, especially noble metals, generally exhibit high electrocatalytic activities relative to their target compounds. Among these materials, silver and copper particles exhibit catalytic activity for $H_2O_2$ reduction [10, 11]. Liu et al. [12] produced silver core-shell on copper particles and noticed that silver provides an increase in the photocatalytic activity of the material. Wang et al. [13] deposited $Ag^0$ particles on the surface of Cu2O particles and doubled the catalytic efficiency against Pironin B after 150 min.

The synthesis of heterostructures formed by the combination of semiconductors offers an important alternative in the search for the combination of the properties of individual components in a single system [14, 15]. These heterostructured compounds have advantages mainly due to the increase of their capacity as charge separators [16], band bending due to Fermi level

equilibration [17, 18], surface properties enhancement [19], and increased gas accessibility [20]. Recently, hybrid nanocatalysts with metal particles on their surface, acting to produce a plasmonic effect, have gained great importance in the study of the decomposition of organic pollutants under visible radiation [10, 21, 22]. The plasmonic effect acts by preventing the electron/hole recombination reaction, increasing the photocatalytic efficiency of the material [23]. The literature [24–27] reports that silver nanoparticles deposited on a semiconductor activates the generation of electron/hole pairs and, consequently, increases the photocatalytic activity under the sunlight or the irradiation of visible light.

Conventional methods of synthesis are made in several steps and generally need calcination. In order to eliminate these problems, the method of sonochemical synthesis has been widely used, as it generally does not need several steps or subsequent calcination. In addition, it is considered a "green" synthesis method [23–26]. Besides, ultrasonic radiation accelerates chemical reactions [28–30]. Ultrasonic radiation is basically based on cavitation, where the formation, growth, and collapse of the bubbles formed by the propagation of the waves in the liquid, cause an increase in temperature and very high local pressure [31–33]. Bubble explosions generate high pressure and temperature of the order of nanoseconds, accompanied by sonoluminescence and mechanical effects [33, 34]. Thus, the yield obtained by the sonochemical synthesis method is greater than that obtained by traditional methods, such as sol-gel and pechini [35, 36].

This work investigated the efficiency of the sonochemical synthesis in obtaining the AgCl/CuO heterostructures and obtaining Ag nanoparticles on the surface of the particles without the need for another process. In addition, we also investigated the changes promoted by the synthesis route change and the AgCl/CuO ratio in the photocatalytic properties under UV-Vis radiation and sunlight, photoluminescent properties, and antimicrobial activity against the bacteria *S. aureus* and *E. coli*.

## Materials and Methods

### Synthesis AgCl/CuO

The AgCl/CuO powders were obtained by a sonochemical method in the Branson 102C tip, operating at a frequency of 20 kHz, through three distinct routes. The heterostructures were obtained in 2 M proportions, AgCl 1:1 CuO (11R1, 11R2, and 11R3), and AgCl 2:1 CuO (21R1, 21R2, and 21R3). For the production of AgCl, $AgNO_3$ (synth, 99%) and NaCl (Dynamic LTDA, 99%) were used, and for the CuO, $Cu(NO_3)_2.2.5H_2O$ (Alfa Aesar, 98%) and $NH_4OH$ (Synth) were stoichiometrically weighed. These were dissolved in 100 mL of distilled water for the preparation of the solutions, and the PVP was added, in a ratio of 1:1 with the nitrates, for a better morphological control. For comparison purposes, AgCl and CuO particles were synthesized in isolation, maintaining the ratio of 1:1, for 30 min. The three routes of synthesis used are illustrated in Fig. 1. All AgCl/CuO compounds were synthesized at room temperature.

### Characterization

AgCl/CuO phase compositions were investigated in a Shimadzu diffractometer (XRD-6000) using CuK$\alpha$ radiation (0.15418 Å). Scanning electron microscopy (SEM) was used to observe the particle morphology. The photocatalytic

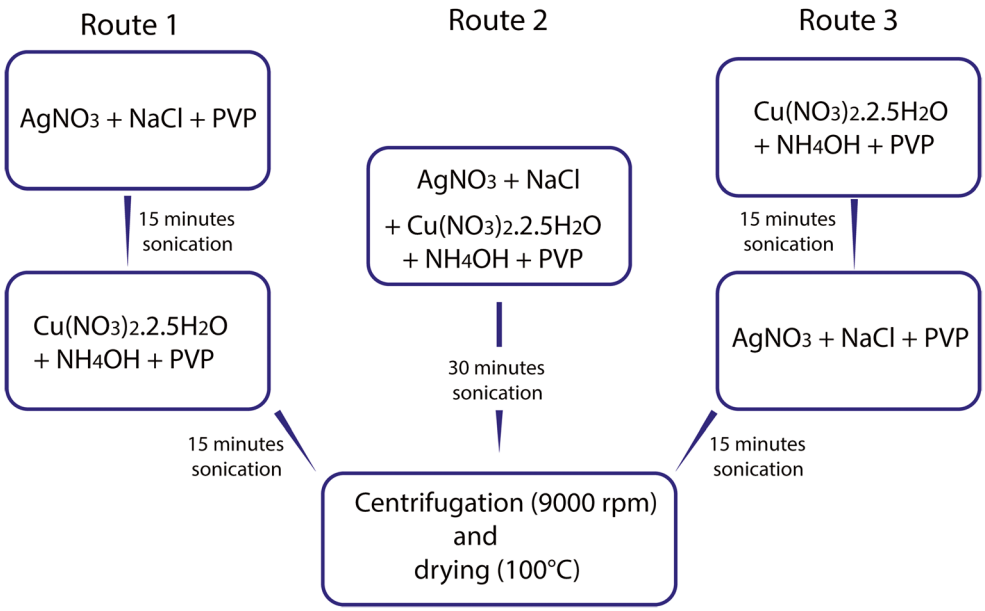


**Fig. 1** Schematic figure of syntheses routes used to obtain AgCl/CuO heterostructures

properties of the samples were tested (as a catalyst) for the degradation of methylene blue dye (MB) with molecular formula [C16H18ClN3S] (99.5% purity, Mallinckrodt) in aqueous solution under UV-Vis illumination and sunlight. The tests were performed on a quartz cylinder containing 50 mL of methylene blue solution (10−5 mol/L concentration) and 0.05 g of material powder. The UV-Vis light test was performed in a reactor containing six UVC lamps (Philips TVU, 15 W, with maximum intensity of 254 nm = 4.9 eV). The test under sunlight occurred outdoors, between 10:00 and 14:00 h, period of higher solar incidence. UV-Vis spectroscopy was performed on Shimadzu equipment (UV-2600), with a wavelength range of 200 to 800 nm and programmed for the diffuse reflectance mode, where from these results, the band gap energy (Egap) was determined using the Wood and Tauc Equation [37]. The antimicrobial activity of the AgCl/CuO particles were tested against *Staphylococcus aureus* (gram-positive) and *Escherichia coli* (gram-negative) bacteria by measuring the inhibition halo (disk diffusion method). This test is established as a standard by the NCCLS (National Committee for Clinical Laboratory Standards). A solution containing the AgCl/CuO particles was deposited on a filter disc with 6 mm diameter, which was deposited in the bacterial inoculum (1 × 108 CFU/mL). The pH of the culture medium remained between 7.2 and 7.4 and the plates were incubated for 24 h at 37 °C in a bacteriological oven. For comparative purposes, the specific antibiotic test (Vancomycin for *S. aureus* and Gentamicin for *E. coli*) was performed.

## Results and Discussions

The XRD technique was used to determine the purity and crystalline structure of the material synthesized by the sonochemical method. Figure 2a, b shows the XRD diffractograms obtained for the three synthetic routes in the ratios AgCl 1:1 CuO and AgCl 2:1 CuO, respectively.

The diffraction peaks for the AgCl and CuO phases are in agreement with ICSD 64734 and ICSD 92365, having cubic (Fig. 3a) and monoclinic structures (Fig. 3b), respectively. Chen et al. [22] synthesized AgCl nanoparticles by a sonochemical method for 30 min and also obtained the phase referring to the ICSD 64734. The cubic structure, related to AgCl, can be confirmed by the diffraction peaks at 2θ angles of 27.825°, 32.238°, and 46.237° for the planes (111), (200), and (220), respectively.

According to the XRD patterns obtained in Fig. 2a, b, the AgCl/CuO powders exhibit a crystalline and orderly structure at long range. These results show that through the sonochemical method it is possible to obtain the material without several steps or future calcination. There was no formation of secondary phases. Liu et al. [21] synthesized nanoparticles of CuO by hydrothermal method, at 80 °C for 12 h, and obtained a monoclinic phase structure equal to that obtained in this study by means of sonochemical for 30 min.

Using the UnittCell-97 Maud software [36], the Rietveld refinement of the diffractograms obtained from the AgCl/CuO heterostructures was performed through the three different routes. Tables 1 and 2 show the values obtained for the crystallite size, phase in volume percentage, lattice parameters, angle β, and volume of each phase.

The lattice parameter values, and consequently the volume of the unit cells for the AgCl/CuO heterostructure, were very close to the patterns ICSD 64734 and ICSD 92365, respectively. Chen et al. [22] synthesized particles of AgCl, by sonochemical method, with network parameter $a = 5.537$ Å and volume of 169.75 Å$^3$, close to the one found in this work. Souza et al. [38] obtained CuO particles by the electrical heating of resistors, with lattice parameters $a = 4.664$ Å, $b = 3.411$ Å, $c = 5.115$ Å, and $\beta = 99.41°$, with a volume of 80.28 Å$^3$, also compatible with those obtained in this work. Table 1 shows that the subsequent synthesis of CuO (route 1) promote the increase of lattice parameter $a$ and reduction of parameters $b$ and $c$. Route 2 promote the increase of crystallite size of AgCl particles, whereas in CuO this increase is observed when produced by route 3. In addition, route 2

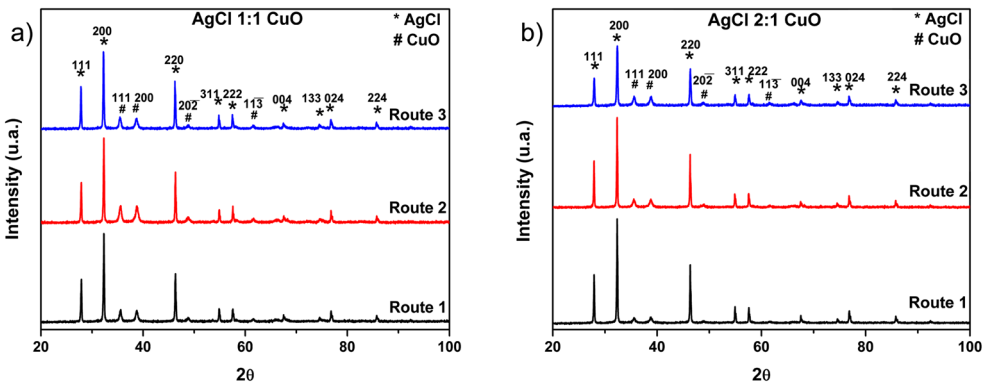


**Fig. 2** XRD pattern of the AgCl/CuO particles obtained by the sonochemical method

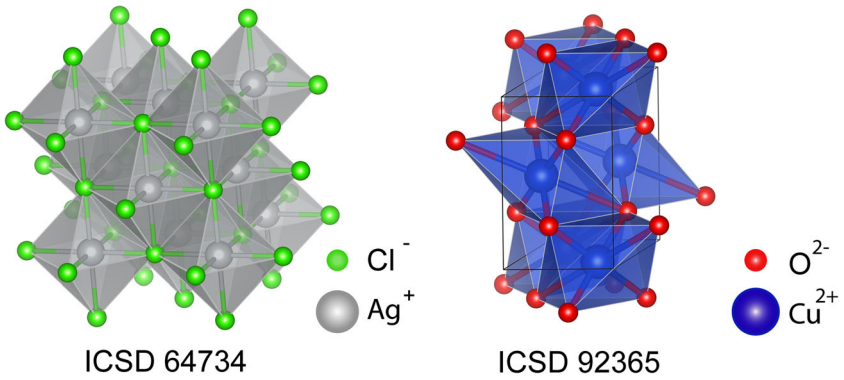


**Fig. 3** Polyhedral representation of structures referring to **a** ICSD 64734 and **b** ICSD 92365

generates a lower percentage of AgCl phase in relation to CuO, contrasting in the worst result of photocatalysis in relation to the other routes.

Figure 4a, c shows the morphology of AgCl and CuO particles obtained by scanning electron microscopy (SEM). Figure 4b, d shows, respectively, the particle size distribution for AgCl and CuO. AgCl presents an irregular aspect and some cubic particles, with a deposition of metallic silver nanoparticles on surface, whereas the CuO particles present a leaf-like morphology. Figure 5 shows the distribution of the particles in AgCl/CuO heterostructure. The variation of the proportion of reagents and the route used did not provide morphological changes in the particles. Figure 4e shows EDS spectrum of a silver particle on the surface of the AgCl particle, obtaining the peaks related to Lα1 (2.984 keV), Lβ1 (3.151 keV), and Lβ2 (3.348 keV), which are characteristic of silver. Chen et al. [22] also observed the formation of metallic silver on the surface of AgCl particles. Pang et al. [39] mentioned that a uniform and controlled morphology increases the coefficient of light absorption, increasing the number of active sites, improving the photocatalytic properties of materials. Still according to Pang et al. [39], for AgCl/Ag, the cubic morphology is better suited for methyl orange catalysis.

The different types of defects in the structure of the material promote the formation of different intermediate levels between the valence and conduction bands [40]. Thus, these defects promote changes in the electronic structure, affecting the optical properties of the material. Table 3 shows the absorption spectrum in the UV-Vis region of the heterostructures and the isolated materials, respectively. The optical gap was obtained by extrapolating the linear region of the curve according to the Wood and Tauc method [37].

According to Table 3, CuO show less Egap than AgCl. Nemade et al. [41] synthesized CuO nanoparticles by varying the concentration of hexamethylenetetramine, obtaining an Egap = 1.24 eV, very similar to the one found in this work. Table 3 also shows that even with the variation of the route and the proportion of the heterostructures, the Egap remains almost constant, with an average value of 1.44 eV, being slightly higher or pure CuO (1.32 eV) and lower than AgCl (2.8 eV). The lower values of Egap are wished due to the possibility of generating electron/hole pairs with higher wavelength radiation, such as visible light.

Figures 6 and 7 show the variation of the methylene blue concentration by the time under UV-Vis radiation and sunlight for the isolated materials (AgCl and CuO) and, for the heterostructure (AgCl/CuO), respectively. The test was executed in triplicate for a more credible results and the curve of the variation of C/Co versus time shows the mean value. The MB curve was obtained without the presence of a semiconductor. Zhang et al. [42] showed that the addition of silver to the copper substrate doped with titanium dioxide (Cu-TiO2)

**Table 1** Lattice parameters and angle β for heterostructure obtained by the three routes of synthesis

| Sample | | Parameter CuO | | | | Parameter AgCl |
|---|---|---|---|---|---|---|
| | | *a* (Å) | *b* (Å) | *c* (Å) | *β* (°) | a (Å) |
| AgCl 1:1 CuO | Route 1 | 4.6949 | 3.4310 | 5.1366 | 99.3778 | 5.5509 |
| | Route 2 | 4.6843 | 3.4275 | 5.1408 | 99.4443 | 5.5484 |
| | Route 3 | 4.6840 | 3.4340 | 5.1385 | 99.3229 | 5.5492 |
| AgCl 2:1 CuO | Route 1 | 4.6960 | 3.4286 | 5.1335 | 99.4349 | 5.5500 |
| | Route 2 | 4.6916 | 3.4306 | 5.1409 | 99.4315 | 5.5512 |
| | Route 3 | 4.6840 | 3.4340 | 5.1385 | 99.3229 | 5.5492 |
| ICSD 64734 | | – | – | – | – | 5.549 |
| ICSD 92365 | | 4.6844 | 3.4192 | 5.1231 | 99.76 | – |

**Table 2** Crystallite size, percentage of volume phase, and volume of the unit cells for the heterostructures obtained by three routes

| Sample | | Dcrys (nm) | | Phase in volume (%) | | V (Å$^3$) | |
|---|---|---|---|---|---|---|---|
| | | AgCl | CuO | AgCl | CuO | AgCl | CuO |
| AgCl 1:1 CuO | Route 1 | 168.78 | 23.71 | 46.19 | 53.80 | 171.03 | 82.74 |
| | Route 2 | 206.68 | 22.05 | 34.74 | 65.25 | 170.80 | 82.53 |
| | Route 3 | 197.26 | 34.50 | 50.88 | 59.11 | 170.88 | 82.65 |
| AgCl 2:1 CuO | Route 1 | 210.92 | 17.47 | 61.47 | 38.52 | 170.95 | 82.65 |
| | Route 2 | 261.90 | 21.78 | 51.23 | 48.76 | 171.06 | 82.74 |
| | Route 3 | 197.26 | 34.50 | 60.88 | 39.11 | 170.88 | 82.65 |

increases its photocatalytic activity on the methylene blue dye due to a decrease in the electron/hole recombination rate, resulting in a higher amount of electrons for transition. According to Woo et al. [43], the impediment of electron/hole recombination provide more electrons free for the transition from the valence band to the conduction band, favoring photocatalysis. In addition, AgCl can generate °Cl which is a strong oxidizing species [44].

The photocatalytic results (Figs. 6 and 7) show that UV-Vis radiation has a higher methylene blue degradation power than visible light, but with the addition of the catalyst, solar radiation acts more efficiently than UV-Vis. According to Teixeira et al. [45], the rate of photocatalytic degradation is independent of light intensity for systems having high illumination. That is, if the catalyst is sufficiently illuminated (absorbed energy greater than Egap), the generation of $e^-/h^+$ pairs must be independent of the radiation source. Since the energy supplied in both cases (sunlight and UV-Vis) is higher than Egap of the isolated materials and the heterostructures (shown in Table 3), the generation of the $e^-/h^+$ pairs occurs efficiently. However, the higher the illumination rate, the more frequent the recombination of $e^-/h^+$ pairs will be. According to Muruganandham et al. [46], the increase in light intensity results in an increase in the rate of degradation of the organic compounds, in which a linear dependence is observed at low intensities, while at high intensities this behavior is not maintained, and the rate of degradation becomes be a function of the square root of the intensity of light. Ollis et al. [47] emphasized that there are two important concepts in the photocatalytic reactions, quantum yield, and photoefficiency. The former deals with the photons absorbed and used for photoexcitation, and the second deals with the reaction rate observed. The photonic efficiency is higher at low luminous intensities [48]. Figures 4 and 5 also show that $Ag^0$ formation

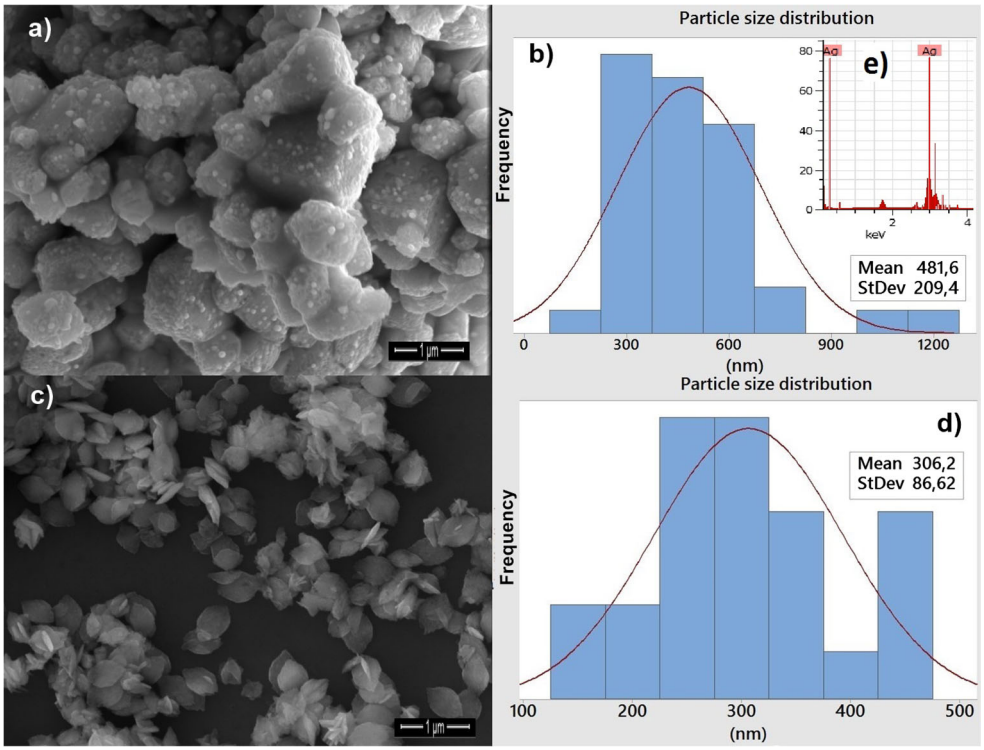


**Fig. 4** Images obtained by SEM for **a** AgCl and **b** CuO

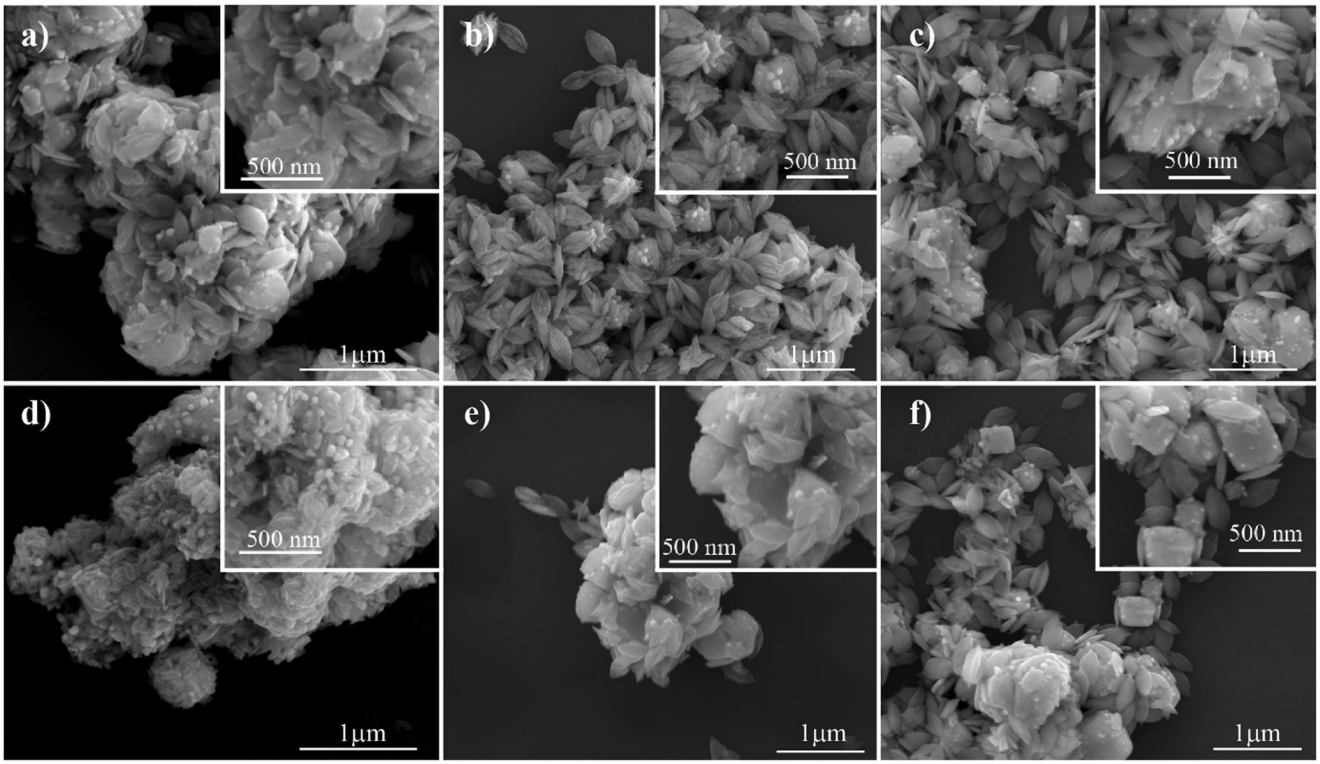


**Fig. 5** Images obtained by SEM for the heterostructures AgCl 1:1 CuO **a** route 1, **b** route 2, and **c** route 3 and AgCl 2:1 CuO **d** route 1, **e** route 2, and **f** route 3

occurs only on the surface of the AgCl particles, causing them to act in the production of the plasmonic effect, increasing the photocatalytic activity of the material. Figure 5 shows that routes 1 and 3 present a more homogeneous distribution of the $Ag^0$ nanoparticles on the surface of the particles, resulting in an optimization of the plasmonic effect, thus increasing the photocatalytic activity [49, 50]. In addition, as shown in Table 2, route 2 presents less amount of AgCl in relation to the others, providing less photocatalytic activity for the heterostructure.

Figure 8a–c shows the photoluminescence curves for the AgCl and CuO compounds and for the heterostructures in the ratios AgCl 1:1 CuO and AgCl 2:1 CuO, respectively. The PL curves presented a broadband in the typical photoluminescent emission spectrum of systems in which the relaxation processes occur in several different ways, involving different intermediate states in the gap of the material [48]. According to this behavior, the PL emission spectra of the investigated heterostructures were decomposed using a Gaussian function with three components. With these decompositions, it may be determined how much each color contributes in the emission. Figure 9 shows the decompositions of the PL curves with the relative percentage of the corresponding color and its maximum peak. Each color in the electromagnetic spectrum represents a set of different electronic transitions and is related to a specific structural arrangement.

Chen et al. [51] observed that silver particles have an absorption band at 450 nm before undergoing UV radiation. Figure 9a shows that the heterostructure produced by route 1 showed displacement in the absorption band to the violet region, a fact that is associated with the later synthesis of CuO related to the AgCl. According to Fig. 9b, c, it can be seen that routes 2 and 3 show some absorption around the blue color, but in route 2, where the synthesis occurs simultaneously, copper acts in a detrimental way to the photoluminescence of the heterostructure, as shown Fig. 8b. Figure 8c illustrates the effect of silver on photoluminescence, where even being synthesized together with copper, its greater amount increases the photoluminescent activity. Botelho et al. [52] obtained $Ag_3PO_4$ particles with maximum emission at 444 nm in the blue region. The increase in amount of silver is also noticeable

**Table 3** Egap obtained by extrapolation of the linear region of the absorption spectrum according to the Tauc method in the UV-Vis region for the AgCl/CuO heterostructures

| Sample | | Egap (eV) |
|---|---|---|
| AgCl 1:1 CuO | Route 1 | 1.45 |
| | Route 2 | 1.44 |
| | Route 3 | 1.43 |
| AgCl 2:1 CuO | Route 1 | 1.45 |
| | Route 2 | 1.45 |
| | Route 3 | 1.40 |
| AgCl | | 2.80 |
| CuO | | 1.32 |

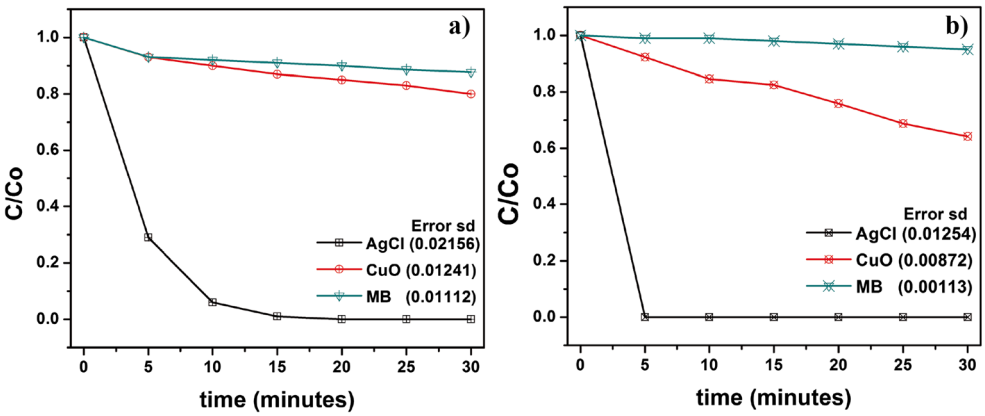


**Fig. 6** Variation of the methylene blue degradation as a function of the time for AgCl and CuO **a** under UV-Vis radiation and **b** sunlight

in route 1, where it provides a shift of the band to around blue. Figure 9d–f illustrates the displacement of the bands to greater wavelengths. Increasing the amount of AgCl in route 1 causes the material to lose its contribution in the ultraviolet region and makes it contribute to the green region of the spectrum. The routes 2 and 3 of synthesis show the increase of the influence of the blue component and a reduction of the others. The effects provided by the Cu occur due to its bivalence, where it acts to reduce the number of holes ($h^+$) and, therefore, damages the photocatalytic and photoluminescent properties of the heterostructures. Oliveira et al. [53] showed that the addition of copper to the structure of $CaTiO_3$ ($CaCu_3Ti_4O_{12}$) significantly decreased the photoluminescence of the material.

The antimicrobial activity was tested against the bacteria *Staphylococcus aureus* (gram-positive) and *Escherichia coli* (gram-negative). The antibiotics Vancomycin (*S. aureus*) and Gentamicin (*E. coli*) were used for control. The diffusion disc technique was used, in which the result is determined by the inhibition halo formed around the sample. Initially, the pure samples were used to determine the best concentration to be used in the heterostructure. The AgCl samples had concentrations of 1, 2, 4, 5, and 10 mg/mL. While the CuO samples varied in 5 and 10 mg/mL. Table 4 shows the inhibition halos formed by these materials.

Table 4 shows that CuO samples did not form an inhibition halo and that the halos formed by the AgCl samples showed

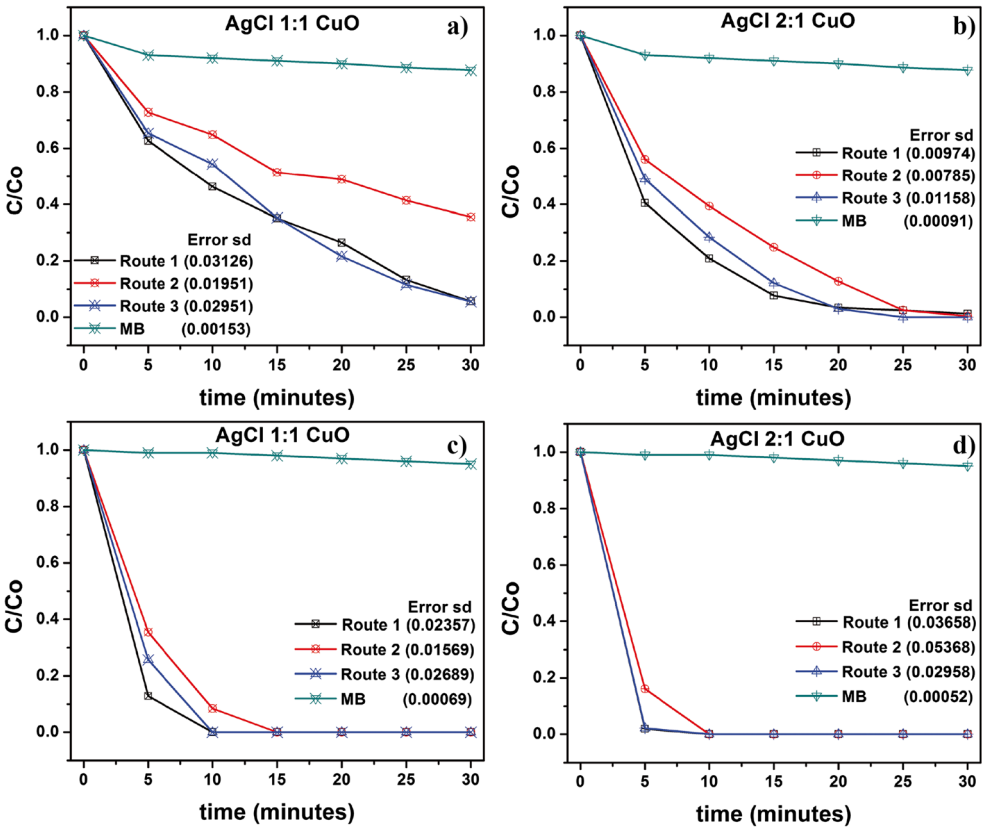


**Fig. 7** Variation of the methylene blue degradation as a function of the time for **a** AgCl 1:1 CuO, **b** AgCl 2:1 CuO under UV-Vis radiation, and **c** AgCl 1:1 CuO, **d** AgCl 2:1 CuO under sunlight

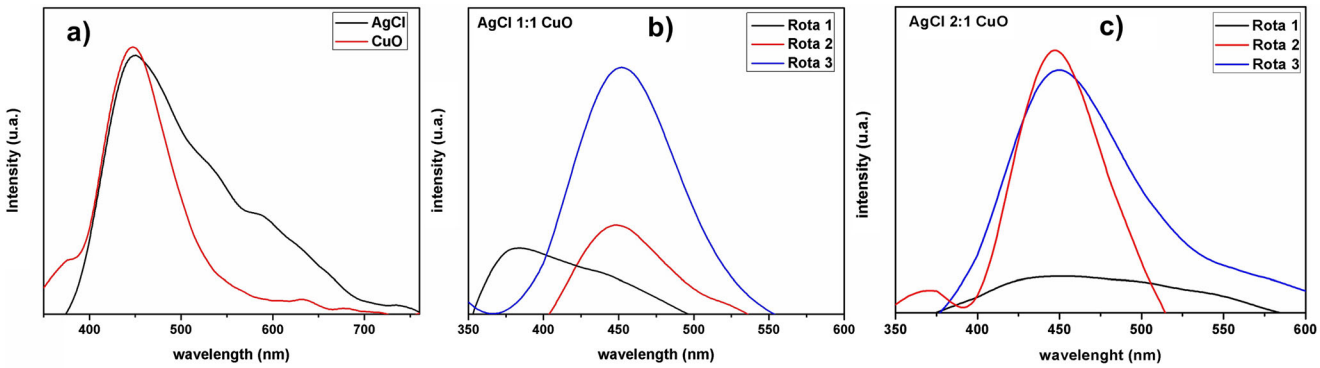


**Fig. 8** Photoluminescence for compounds **a** AgCl and CuO and heterostructures obtained in proportions, **b** AgCl 1:1 CuO, and **c** AgCl 2:1 CuO

no significant difference. With the results of Table 4, the concentration of 5 mg/mL for the AgCl/CuO heterostructure was established. Figure 10 shows the inhibition halos formed by these heterostructures against *S. aureus* and *E. coli* bacteria.

The AgCl/CuO heterostructures presented antimicrobial activity superior to the isolated AgCl and CuO compounds, showing that there are positive effects of the interaction between the compounds. Neto et al. [54] showed through an experimental design that increasing the amount of PVP promotes a reduction in the size of the AgCl particles. In addition, it provides an increase in the photocatalytic properties against the methylene blue dye. However, because it is a polymer, it can act negatively in the antimicrobial activity [55, 56]. Sheehy et al. [57] synthesized silver nanoparticles stabilized with PVP and performed a study varying their concentration from 10 to 100 ppm and, for all concentrations, it did not obtained the formation of inhibition halos against *E. coli* bacteria. The particle size is an important factor on antimicrobial activity, in which the larger its surface area, the better the results obtained [53]. The AgCl/CuO particles had no nanometric structure, and it may be the cause of their low activity. Jurek et al. [55] observed that the increase in Ag-Pt/TiO2 particle size negatively influences the antimicrobial properties against *E. coli* and *S. aureus* bacteria. Bera et al. [56] studied the antimicrobial activity of silver nanoparticles, varying their size, and reported that their increase impairs such

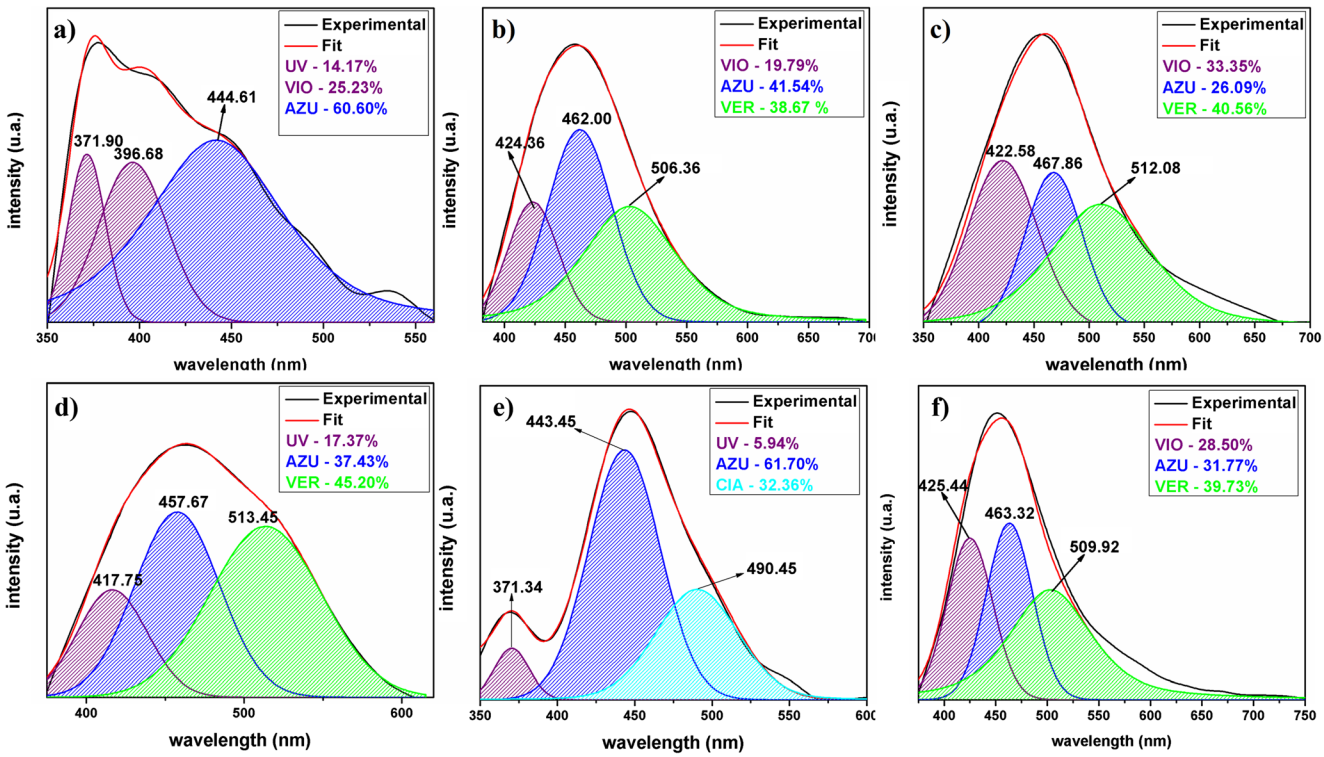


**Fig. 9** Deconvolution of the PL emission curves of the heterostructures obtained in the proportions AgCl 1:1 CuO by the **a** route 1, **b** route 2, and **c** route 3 and AgCl 2:1 CuO by the **d** route 1, and **e** route 2 and **f** route 3. UV = ultraviolet component, VIO = violet component, AZU = blue component, CIA = cyano component, VER = green component

**Table 4** Inhibition halo diameter (mm) for AgCl and CuO varying the concentration

| Sample | | Inhibition halo diameter (mm) for *Staphylococcus aureus* | Inhibition halo diameter (mm) for *Escherichia coli* |
|---|---|---|---|
| AgCl | 1 mg/mL | 9.22 ± 0.016 | 9.45 ± 0.091 |
| | 2 mg/mL | 9.34 ± 0.070 | 9.18 ± 0.307 |
| | 4 mg/mL | 9.93 ± 0.026 | 9.82 ± 0.145 |
| | 5 mg/mL | 9.58 ± 0.092 | 9.76 ± 0.0351 |
| | 10 mg/mL | 10.11 ± 0.138 | 9.87 ± 0.183 |
| CuO | 5 mg/mL | 6 | 6 |
| | 10 mg/mL | 6 | 6 |
| Vancomycin | | 18.33 ± 0.023 | – |
| Gentamicin | | – | 18.30 ± 0.017 |

activity against *S. epidermidis*, *B. megaterium*, *E. coli*, and *P. aeruginosa* bacteria.

## Conclusion

The sonochemical method was shown to be simple and efficient to obtain the heterostructures, not requiring a subsequent calcination. The variation in the ratio and in the synthesis routes did not change the phases of the heterostructure (AgCl/CuO). It was noticed that the alteration of the synthesis route provided different photocatalytic behaviors, where routes 1 and 3 presented similar results and route 2 presented the worst performance when irradiated by sunlight and UV-Vis. The AgCl/CuO heterostructure showed superior photocatalytic activity when irradiated with sunlight, related to UV-Vis, presenting a reduction of at least 55% in the degradation of methylene blue. The increase in the ratio of AgCl provided an acceleration in the reduction of the methylene blue concentration. The particles of AgCl presented metallic silver deposited on their surface, where these particles act producing a plasmonic effect, positively influencing the photocatalytic activity of the material. Simultaneous synthesis and addition of CuO following the silver causes a reduction in the photoluminescent properties, a fact that loses relevance when the ratio AgCl/CuO is changed from 1:1 to 2:1. SEM images show the cubic morphology of AgCl particles, whereas CuO particles show a leaf-like morphology. CuO showed no antimicrobial activity against the *E. coli* and *S. aureus* bacteria, whereas the AgCl showed a low activity compared to the reference. The AgCl/CuO heterostructure showed higher antimicrobial activity than the AgCl, showing interaction among the compounds.

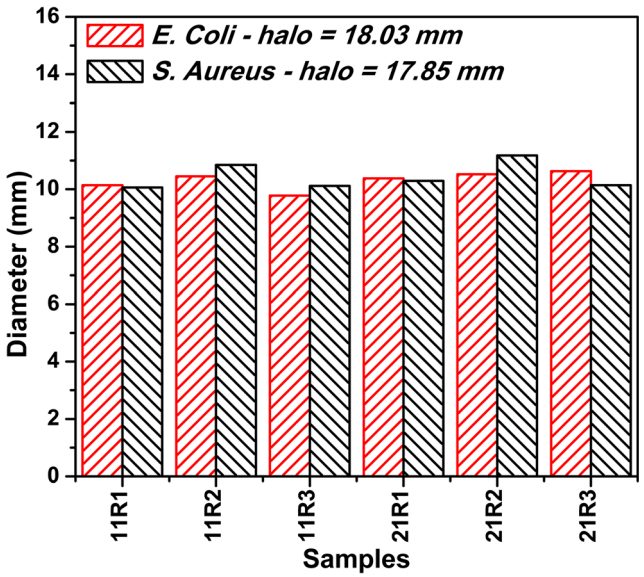


**Fig. 10** Antimicrobial activity of AgCl/CuO heterostructure against *S. aureus* (a) and *E. coli* (b) bacteria

**Acknowledgements** The authors thank the financial support of the Brazilian research financing institutions: CAPES, CNPq No. 402127/2013-7, and FAPESP 2013/07296-2.

## References

1. Ananth A, Dharaneedharan S, Heo MS, Mok YS (2015) Copper oxide nanomaterials: synthesis, characterization and structure-specific antibacterial performance. Chem Eng J 262:179–188
2. Dizaj SM, Lotfipour F, Barzegar-Jalali M, Zarrintan MH, Adibkia K (2014) Antimicrobial activity of the metals and metal oxide nanoparticles. Mater Sci Eng C Mater Biol Appl 44:278–284
3. Reitz JB, Solomon EI (1998) Propylene oxidation on copper oxide surfaces: electronic and geometric contributions to reactivity and selectivity. J Am Chem Soc 120:11467–11478
4. Ramírez-Ortiz J, Ogura T, Medina-Valtierra J, Acosta-Ortiz SaE, Bosch P, Antonio de los Reyes J, Lara VH (2001) A catalytic application of Cu2O and CuO films deposited over fiberglass. Appl Surf Sci 174:177–184
5. Sun J-H, Dong S-Y, Wang Y-K, Sun S-P (2009) Preparation and photocatalytic property of a novel dumbbell-shaped ZnO microcrystal photocatalyst. J Hazard Mater 172:1520–1526
6. Yola ML, Eren T, Atar N, Wang S (2014) Adsorptive and photocatalytic removal of reactive dyes by silver nanoparticle-colemanite ore waste. Chem Eng J 242:333–340
7. Shamsipur M, Farzin L, Amouzadeh Tabrizi M, Sheibani S (2017) Functionalized Fe3O4/graphene oxide nanocomposites with

hairpin aptamers for the separation and preconcentration of trace Pb2+ from biological samples prior to determination by ICP MS. Mater Sci Eng C Mater Biol Appl 77:459–469
8. Atar N, Eren T, Yola ML, Gerengi H, Wang S (2015) Fe@Ag nanoparticles decorated reduced graphene oxide as ultrahigh capacity anode material for lithium-ion battery. Ionics 21:3185–3192
9. Ibănescu M, Muşat V, Textor T, Badilita V, Mahltig B (2014) Photocatalytic and antimicrobial Ag/ZnO nanocomposites for functionalization of textile fabrics. J Alloys Compd 610:244–249
10. Welch CM, Banks CE, Simm AO, Compton RG (2005) Silver nanoparticle assemblies supported on glassy-carbon electrodes for the electro-analytical detection of hydrogen peroxide. Anal Bioanal Chem 382:12–21
11. Wang L, Zhu H, Hou H, Zhang Z, Xiao X, Song Y (2012) A novel hydrogen peroxide sensor based on Ag nanoparticles electrodeposited on chitosan-graphene oxide/cysteamine-modified gold electrode. J Solid State Electrochem 16:1693–1700
12. Liu X, Li Z, Zhao C, Zhao W, Yang J, Wang Y, Li F (2014) Facile synthesis of core-shell CuO/Ag nanowires with enhanced photocatalytic and enhancement in photocurrent. J Colloid Interface Sci 419: 9–16
13. Wang Z, Zhao S, Zhu S, Sun Y, Fang M (2011) Photocatalytic synthesis of M/Cu2O (M = Ag, Au) heterogeneous nanocrystals and their photocatalytic properties. CrystEngComm 13:2262–2267
14. Chen Y, Yu L, Feng D, Zhuo M, Zhang M, Zhang E, Xu Z, Li Q, Wang T (2012) Superior ethanol-sensing properties based on Ni-doped SnO2 p–n heterojunction hollow spheres, Sensors & Actuators: B. Chemical 166-167:61–67
15. Kaur N, Zappa D, Ferroni M, Poli N, Campanini M, Negrea R, Comini E (2018) Branch-like NiO/ZnO heterostructures for VOC sensing. Sensors Actuators B Chem 262:477–485
16. Yu X, Zhang G, Cao H, An X, Wang Y, Shu Z, An X, Hua F (2012) ZnO@ZnS hollow dumbbells-graphene composites as high-performance photocatalysts and alcohol sensors. New J Chem 36: 2593–2598
17. Kusior A, Radecka M, Rekas M, Lubecka M, Zakrzewska K, Reszka A, Kowalski BJ (2012) Sensitization of gas sensing properties in TiO2/SnO2 Nanocomposites. Procedia Engineering 47: 1073–1076
18. Chen A, Bai S, Shi B, Liu Z, Li D, Liu CC (2008) Methane gas-sensing and catalytic oxidation activity of SnO2–In2O3 nanocomposites incorporating TiO2. Sensors Actuators B Chem 135:7–12
19. Liangyuan C, Shouli B, Guojun Z, Dianqing L, Aifan C, Liu CC (2008) Synthesis of ZnO–SnO2 nanocomposites by microemulsion and sensing properties for NO2. Sensors Actuators B Chem 134: 360–366
20. Zeng Y, Bing Y-f, Liu C, Zheng W-t, Zou G-t (2012) Self-assembly of hierarchical ZnSnO3-SnO2 nanoflakes and their gas sensing properties. Trans Nonferrous Metals Soc China 22:2451–2458
21. Liu J, Jin J, Deng Z, Huang S-Z, Hu Z-Y, Wang L, Wang C, Chen L-H, Li Y, Van Tendeloo G, Su B-L (2012) Tailoring CuO nanostructures for enhanced photocatalytic property. J Colloid Interface Sci 384:1–9
22. Chen D, Yoo SH, Huang Q, Ali G, Cho SO (2012) Sonochemical synthesis of Ag/AgCl nanocubes and their efficient visible-light-driven photocatalytic performance. Chem Eur J 18:5192–5200
23. Sayyed IA, Thakur VV, Nikalje MD, Dewkar GK, Kotkar SP, Sudalai A (2005) Asymmetric synthesis of aryloxypropanolamines via OsO4-catalyzed asymmetric dihydroxylation. Tetrahedron 61: 2831–2838
24. Li Z, Chen X, Xue Z-L (2013) Microwave-assisted hydrothermal synthesis of cube-like Ag-Ag2MoO4 with visible-light photocatalytic activity. SCIENCE CHINA Chem 56:443–450
25. Guo J-F, Ma B, Yin A, Fan K, Dai W-L (2011) Photodegradation of rhodamine B and 4-chlorophenol using plasmonic photocatalyst of Ag–AgI/Fe3O4@SiO2 magnetic nanoparticle under visible light irradiation. Appl Catal B Environ 101:580–586
26. Dai W-L, Xu H, Yang L-X, Luo X-B, Tu X-M, Luo Y (2015) Ultrasonic-assisted facile synthesis of plasmonic Ag@AgCl cuboids with high visible light photocatalytic performance for Rhodamine B degradation. React Kinet Mech Catal 115:773–786
27. Fernandes JPdS, Carvalho BS, Luchez CV, Politi MJ, Brandt CA (2011) Optimization of the ultrasound-assisted synthesis of allyl 1-naphthyl ether using response surface methodology. Ultrason Sonochem 18:489–493
28. Tamuly C, Hazarika M, Das J, Bordoloi M, Borah DJ, Das MR (2014) Bio-derived CuO nanoparticles for the photocatalytic treatment of dyes. Mater Lett 123:202–205
29. Cravotto G, Cintas P (2007) Forcing and controlling chemical reactions with ultrasound. Angew Chem Int Ed 46:5476–5478
30. Brandt CA, da Silva ACMP, Pancote CG, Brito CL, da Silveira MAB (2004) Efficient synthetic method for β-enamino esters using ultrasound. Synthesis 2004:1557–1559
31. Jiang J, Zhang L (2011) Rapid microwave-assisted nonaqueous synthesis and growth mechanism of AgCl/Ag, and its daylight-driven plasmonic photocatalysis. Chem Eur J 17:3710–3717
32. Zhu S, Zhou H, Hibino M, Honma I, Ichihara M (2005) Synthesis of MnO2 nanoparticles confined in ordered mesoporous carbon using a sonochemical method. Adv Funct Mater 15:381–386
33. Bang JH, Suslick KS (2010) Applications of ultrasound to the synthesis of nanostructured materials. Adv Mater 22:1039–1059
34. Kim J, Park C, Kim T-H, Lee M, Kim S, Kim S-W, Lee J (2003) Effects of various pretreatments for enhanced anaerobic digestion with waste activated sludge. J Biosci Bioeng 95:271–275
35. Han J, Fang P, Jiang W, Li L, Guo R (2012) Ag-nanoparticle-loaded Mesoporous silica: spontaneous formation of Ag nanoparticles and mesoporous silica SBA-15 by a one-pot strategy and their catalytic applications. Langmuir 28:4768–4775
36. Lutterotti L (2010) Total pattern fitting for the combined size–strain–stress–texture determination in thin film diffraction. Nucl Instrum Methods Phys Res, Sect B 268:334–340
37. Wood DL, Tauc J (1972) Weak absorption tails in amorphous semiconductors. Phys Rev B 5:3144–3151
38. Souza JA, Criado D, Zuniga A, Miranda VN, Ramirez FEN, Masunaga SH, Jardim RF (2013) Enhanced ferromagnetism in CuO nanowires on the top of CuO nanograins. J Appl Phys 114: 173907
39. Pang Y, Song L, Chen C, Ge L (2017) Cu(II) cocatalyst modified Ag@AgCl cubic cages with enhanced visible light photocatalytic activity and stability. J Mater Sci Mater Electron 28:12572–12579
40. Cavalcante LS, Batista FMC, Almeida MAP, Rabelo AC, Nogueira IC, Batista NC, Varela JA, Santos MRMC, Longo E, Siu Li M (2012) Structural refinement, growth process, photoluminescence and photocatalytic properties of (Ba1-xPr2x/3)WO4 crystals synthesized by the coprecipitation method. RSC Adv 2:6438–6454
41. Nemade KR, Waghuley SA (2012) Study of optical band gap of CuO using Fermi's golden rule. J Phys Conf Ser 365:012018
42. Zhang W, Liu Y, Yu B, Zhang J, Liang W (2015) Effects of silver substrates on the visible light photocatalytic activities of copper-doped titanium dioxide thin films. Mater Sci Semicond Process 30:527–534
43. Lee WK, Kim EJ, Hahn SH (2010) Structural and photocatalytic properties of TiO2/SiOx/TiOx multi-layer prepared by electron-beam evaporation method. Vacuum 85:30–33
44. Gamage J, McEvoy W, Cui ZZ (2014) Synthesis and characterization of Ag/AgCl–activated carbon composites for enhanced visible light photocatalysis. Appl Catal B Environ 144:702–712
45. W.F.J. C. P. A. B. Teixeira, Processos oxidativos avançados: conceitos teóricos. Caderno temático, 2004

46. Muruganandham M, Swaminathan M (2006) Photocatalytic decolourisation and degradation of reactive orange 4 by TiO2-UV process. Dyes Pigments 68:133–142
47. Peral J, Ollis DF (1992) Heterogeneous photocatalytic oxidation of gas-phase organics for air purification: acetone, 1-butanol, butyraldehyde, formaldehyde, and m-xylene oxidation. J Catal 136:554–565
48. Motta FV, Marques APA, Espinosa JWM, Pizani PS, Longo E, Varela JA (2010) Room temperature photoluminescence of BCT prepared by complex polymerization method. Curr Appl Phys 10:16–20
49. Kumar D, Singh S, Khare N (2018) Plasmonic Ag nanoparticles decorated NaNbO3 nanorods for efficient photoelectrochemical water splitting. Int J Hydrog Energy 43:8198–8205
50. Sadrieyeh S, Malekfar R (2018) Photocatalytic performance of plasmonic Au/Ag-TiO2 aerogel nanocomposites. J Non-Cryst Solids 489:33–39
51. Chen Y, Yang T, Pan H, Yuan Y, Chen L, Liu M, Zhang K, Zhang S, Wu P, Xu J (2014) Photoemission mechanism of water-soluble silver nanoclusters: ligand-to-metal–metal charge transfer vs strong coupling between surface plasmon and emitters. J Am Chem Soc 136:1686–1689
52. Botelho G, Andres J, Gracia L, Matos LS, Longo E (2016) Photoluminescence and photocatalytic properties of Ag3PO4 microcrystals: an experimental and theoretical investigation. ChemPlusChem 81:202–212
53. Oliveira LH, Paris EC, Avansi W, Ramirez MA, Mastelaro VR, Longo E, Varela JA (2013) Correlation between photoluminescence and structural defects in Ca1+xCu3−xTi4O12 systems. J Am Ceram Soc 96:209–217
54. Neto NFA, Garcia LMP, Longo E, Li MS, Paskocimas CA, Bomio MRD, Motta FV (2017) Photoluminescence and photocatalytic properties of Ag/AgCl synthesized by sonochemistry: statistical experimental design. J Mater Sci Mater Electron 28:12273–12281
55. Zielińska-Jurek A, Wei Z, Wysocka I, Szweda P, Kowalska E (2015) The effect of nanoparticles size on photocatalytic and antimicrobial properties of Ag-Pt/TiO2 photocatalysts. Appl Surf Sci 353:317–325
56. Bera RK, Mandal SM, Raj CR (2014) Antimicrobial activity of fluorescent Ag nanoparticles. Lett Appl Microbiol 58:520–526
57. Sheehy K, Casey A, Murphy A, Chambers G (2015) Antimicrobial properties of nano-silver: a cautionary approach to ionic interference. J Colloid Interface Sci 443:56–64